Inactivation of citron kinase inhibits medulloblastoma progression by inducing apoptosis and cell senescence

Citron kinase inactivation inhibits medulloblastoma progression by inducing apoptosis and cell senescence.

Gianmarco Pallavicini[1,2 #], Francesco Sgrò[1 #], Francesca Garello[1], Mattia Falcone[1,3,4], Valeria Bitonto[1], Gaia E. Berto[1,2], Federico T. Bianchi[1,2], Marta Gai[1], Alessandra M.A. Chiotto[1,2], Miriam Filippi[1], Juan C. Cutrin[1], Ugo Ala[1], Enzo Terreno[1], Emilia Turco[1] and Ferdinando Di Cunto[1,2,5 *]

1. Department of Molecular Biotechnology and Health Sciences, University of Turin, Italy.

2. Neuroscience Institute Cavalieri Ottolenghi, University of Turin, Italy.

3. Division of Stem Cells and Cancer, German Cancer Research Center (DKFZ) and DKFZ-ZMBH Alliance, Heidelberg, Germany

4. Heidelberg Institute for Stem Cell Technology and Experimental Medicine (HI-STEM gGmbH), Heidelberg, Germany

5. Department of Neuroscience, University of Turin, Italy.

 # These authors equally contributed to the manuscript.

** Corresponding author. Neuroscience Institute Cavalieri Ottolenghi, Regione Gonzole 10, 10043, Orbassano (TO), Italy. E-mail: ferdinando.dicunto@unito.it. Phone: +39 011 6706616. Fax: +39 011 6706621*

Running title: CITK inactivation inhibits medulloblastoma progression.

Financial support: Associazione Italiana per la Ricerca sul Cancro (AIRC), Grant n. IG17527 to F.D.C; MIUR PhD fellowship to G.P. and V.B.; Fondazione Umberto Veronesi fellowship to F.G.

Keywords: Medulloblastoma, CITK, SHH, Senescence, Apoptosis.

Conflict of interest: The authors declare no potential conflicts of interests.

Abstract

Medulloblastoma (MB) is the most common malignant brain tumor in children. Current treatment for MB, consisting of surgery followed by irradiation of the whole neuraxis and high-dose multi-agent chemotherapy, is only partially effective and is associated with highly invalidating side effects. Therefore, the identification and validation of novel target molecules, capable of contrasting MB growth without disturbing brain development, is needed. Citron kinase protein (CITK), encoded by primary microcephaly gene MCPH17, is required for normal proliferation and survival of neural progenitors. Constitutive loss of CITK leads to cytokinesis failure, chromosome instability and apoptosis in developing brain, but has limited effects on other tissues. On this basis, we hypothesized that CITK could be an effective target for MB treatment. We tested this hypothesis using the MB cell lines DAOY and ONS-76. In these cells, CITK knockdown increases both cytokinesis failure and DNA damage, impairing proliferation and inducing cell senescence and apoptosis via TP53 or TP73. Similar effects were obtained in MB arising in the NeuroD-SmoA1 transgenic mouse model, in which CITK deletion increases apoptotic cells and senescence markers, such as $P21^{CIP1}$, $P27^{KIP1}$ and $P16^{INK4A}$. Most importantly, CITK deletion decreases tumor growth and increases overall survival in these mice, with no apparent side effects. These results suggest that CITK can be a useful molecular target for MB treatment.

Introduction

Medulloblastoma (MB) is the most common malignant brain tumor in children (1). MB has been classified into five subgroups based on histology and into four biological subgroups based on microarray and genomic sequencing technologies: WNT, Sonic Hedgehog (SHH), group 3 and group 4 (2–6). WNT MB are associated with relatively good prognosis, while group 3 and 4, which often show MYC amplification and TP53 mutation, are the most aggressive subtypes (5). Current treatments for MB include surgery followed by irradiation of the whole neuraxis and high-dose multi-agent chemotherapy (7). 5-years survival rate for children with average and high-risk disease, as defined by clinical criteria, is 80% and 60–65%, respectively (8). Therefore, many of the high-risk patients die despite treatment (9). In addition, survivors have significant neurologic and developmental consequences, such as severe cognitive deficits and endocrine disorders (10–15). Thus, novel and more specific therapies are urgently needed. A possible strategy to develop new selective therapies is to directly target molecular pathways altered by driver mutations. SHH subgroup, representing approximately 25% of MB cases, is the better understood MB subtype: it is characterized by mutations of SHH signaling pathway downstream components (PTCH1, SMO, SUFU and GLI2) and it is derived from granule neuron precursors (GNPs) of the cerebellum (16–18). Small-molecule inhibitors of the SHH pathway have been developed and tested in clinical trials (19). However, only a subgroup of these patients respond to treatment and even in these cases resistance rapidly develops (20–22). An alternative strategy for drug development is to target molecules that, despite not being mutated in cancer, are nevertheless required for tumor growth and progression (23). Cancer cells may become specifically dependent on particular non-mutant proteins in consequence of peculiar features of the cells from which they originate and/or of the modifications induced by oncogenic transformation (23).

CITK is a conserved multi-domain protein, containing an AGC-type amino-terminal serine/threonine kinase domain (24,25). CITK is ubiquitously expressed (26) and cell-cycle regulated, with highest levels in G2/M phase of the cell cycle (27). During mitosis, it is first localized to the nucleus (27), it is enriched at spindle poles before anaphase (28), it is concentrated at cleavage furrow and midbody from anaphase to cytokinesis (25). CITK is a specific regulator of abscission at the end of cytokinesis (25,29–32). In addition, it regulates mitotic spindle orientation (33) and it is involved in genomic stability independently of its role in cytokinesis (34). Despite ubiquitous expression, CITK is functionally required *in vivo* only in few cell types, such as neural progenitors (26,35) and male germ cells (36). CITK loss leads to severe microcephaly in rodents (26,37) and humans (38–41). Cells in the affected tissues display cytokinesis failure (26,40), apoptosis (26,36,40) and accumulation of DNA damage (34). Notably, the human CITK microcephaly syndrome, known as MCPH17, can be caused by homozygous kinase-inactivating mutations (40), indicating that catalytic activity is essential for function.

CITK is expressed at high levels in tumors (42–44) and is required for normal growth in tumor cell lines of different origin (45–47). Moreover, CITK knock-down reduces tumor growth in hepatocellular carcinoma cells in xenograft assays (45). These results suggest that CITK could be an interesting target for anti-cancer drug development. However, the effects of CITK inactivation have never been tested in primary tumors. Based on current knowledge (30,48), SHH MB appears to be an ideal tumor type for testing the potential of CITK as a candidate drug target. Indeed, cerebellar GNPs, from which SHH MB develops (16–18), are among the neural progenitors showing highest sensitivity to CITK loss (26). Moreover, MB express high levels of TUBB3 (49), which may increase sensitivity to CITK loss (50). Finally, while CITK is essential for normal brain development, it is not required in normal postnatal tissues (26,34), and therefore its acute inactivation should be associated

with relatively mild side effects.

In this report we analyzed the effects of deleting CITK in SHH MB, using *in vitro* and *in vivo* models, including conditional inactivation in primary tumors. Our results support CITK as a novel drug target for this tumor type.

Materials and methods

Cell culture.

DAOY cells were obtained from ATCC and were cultured according to the ATCC protocol. ONS-76 cells were kindly provided by Luigi Varesio (Gaslini Hospital, Genova) and were cultured in RPMI medium supplemented with 10% fetal bovine serum (FBS) and 1% penicillin/streptomycin (Life Technologies, ThermoFisher, Waltham, MA). For both cell lines, the number of in vitro passages from thawing of the original aliquots to experiments was comprised between 5 and 8. Cells were routinely analyzed for morphological features and tested for Mycoplasma contamination with the following oligonucleotides sequences: MYCO1 5'-ACTCCTACGGGAGGCAGCAGTA-3'; MYCO2: 5'-TGCACCATCTGTCACTCTGTTAACCTC-3'.

Transfection and RNAi.

Previously published CITK double-stranded RNAs (31) and non-targeting siRNA were used (Dharmacon, Lafayette, CO). For knockdown of TP53 and TP73 ONTARGETplus Dharmacon SMART pools were used. D-001810-10 non-targeting pool was used as a negative control. ONS-76 and DAOY cells plated on six-well plates were transfected using 6.25 µl of the required siRNA (20 µM) together with 1.5 µl Lipofectamine 2000 (Invitrogen, Carlsbad, CA), according to the manufacturer's instructions. Efficient knockdown was obtained after 48h.

Lentiviral production.

HEK293T cells were cultured in DMEM supplemented with 10% fetal Calf serum (FCS) and 1% penicillin/streptomycin (Life Technologies, ThermoFisher, Waltham, MA). Lentiviral vector stocks were produced in HEK293T cells by calcium phosphate-mediated transfection as described in (51).

Generation of inducible shRNA cell lines and rescue of CITK expression.

Human CITK-specific shRNA sequences (31) were cloned into pLVTHM vector from Didier Trono's lab (Addgene plasmid #12247, Fig. S1A). For inducible RNAi, cells were transduced with pLV-DsRed-tTRKRAB from Didier Trono lab (Addgene plasmid #12247, Fig. S1A), expanded, and used for transduction with pLVTH-GFP-shRNA lentiviral particles. Next, cells were treated with doxycycline (2 µM) for 12 hours; double $GFP^{+}DsRed^{+}$ cells were sorted by FACSAria (BD biosciences, Franklin Lakes, NJ) and expanded. Cells expressing GFP in the absence of doxycycline were considered “leaky” and removed by a second flow of cytometry sorting. Purified inducible cells showed efficient knockdown after 24h, as determined by western blot analysis. For rescue experiments, Myc-cherry-tagged CITK over-expression constructs encoding kinase-active or kinase-inactive (S222A) proteins previously described (31) were transfected at the same time of doxycycline induction with 10.5 µl of Lipofectamine 2000 (ThermoFisher, Invitrogen, Carlsbad, CA), according to the manufacturer's instructions. Live cells, as assessed by methylene blue staining, were counted after 24h.

Analysis of cell death and proliferation.

For apoptosis detection, 5×10^5 cells were collected, centrifuged at 2,000 rpm for 5 min, and re-suspended in 300 µl of binding buffer. Annexin V FITC (3 µl) was added and mixed. After the addition of 5 µl of propidium iodide (PI) staining solution, the cells were incubated for 15-30 min in the dark at room temperature and analyzed by flow cytometry to detect cell apoptosis. For cell proliferation analysis, $5x10^3$ ONS-76 and DAOY inducible cells

were seeded into twenty-four-well plates and activated using doxycycline (2 µM). Live cells were counted in replica wells each day for six days.

Experimental Animal Work.

Experiments involving samples from mutant and control mice have been performed conforming to the Italian laws on animal experimentation, under permission number 343/2015-PR, released on 08/05/2015 from Italian Ministry of Health, Department of Public Veterinary Health. Adherence to internationally accepted animal well-being standards was further supervised by the veterinary service of the Molecular Biotechnology Centre animal facility.

Xenograft assays.

Subcutaneous MB xenografts were obtained by transplanting in mice DAOY cells expressing control or CITK-targeted shRNAs under doxycycline-inducible control. Four to eight-week old female NOD-SCID mice (Jackson Laboratory) were injected in the flank with $2x10^6$ cells. After 6 weeks, doxycycline (10 mg/ml) was added to drinking water for other 4 weeks. Xenograft tumors were measured every week and tumor volume was estimated as $4\pi r^3 / 3$.

Mouse strains.

The mouse strain containing the 'knockout first' allele of CitK $Cit^{tm1a(KOMP)Wtsi}$, in a C57BL/6 background, was obtained from UC Davis KOMP repository. The Citron kinase conditional knockout allele Cit^{flox} was obtained by crossing $Cit^{tm1a(KOMP)Wtsi}$ mice with the FLP-balancer line $Gt(ROSA)26Sor^{tm2(FLP*)Sor}$, in a C57BL/6J congenic background (The Jackson Laboratory, Bar Harbor, Main). The mouse strains $Gt(ROSA)26Sor^{tm1(cre/ERT2)Tyj}$ (ubiquitously-expressing tamoxifen-inducible ER^{T2}-CRE) and ND2:SmoA1 (expressing the constitutively active point mutant SmoA1 under the Neurod2 promoter in cerebellar

granule cells), both in congenic C57BL/6 background, were obtained from The Jackson Laboratory.

Antibodies

The following antibodies were used: mouse monoclonal anti-Citron (#611377 Transduction Laboratories, BD Biosciences, San Jose, CA, USA), mouse monoclonal anti-Vinculin (#V9131 Sigma-Aldrich); rabbit polyclonal anti-γH2AX (S139) (20E3) (#2577 Cell Signaling Technology, Danvers, MA, USA), mouse monoclonal anti-P27 (#610242 Transduction Laboratories, BD Biosciences, San Jose, CA, USA), rabbit polyclonal anti-cleaved Caspase 3 (#9661S Cell Signaling Technology, Danvers, MA, USA), goat polyclonal anti-cleaved Caspase7 (#sc-6138 Santacruz, Dallas, TX, USA), rabbit polyclonal anti-P21 (#sc-756 Santacruz, Dallas, TX, USA), rabbit polyclonal anti-P16 (#sc-1207 Santacruz, Dallas, TX, USA), mouse monoclonal anti-Ki67 (#ab15580 Abcam, Cambridge, GB), rabbit polyclonal anti-TP53(#sc-6243 Santacruz, Dallas, TX, USA), rabbit polyclonal anti-TP73 (#ab14430 Abcam, Cambridge, GB), mouse monoclonal anti-αTubulin (#T5168 Sigma-Aldrich, Saint Louis, MS, USA), rabbit polyclonal anti-βactin (#A2066 Sigma-Aldrich).

Western blotting

Cell lines and tissues were lysed in RIPA buffer (1% NP40, 150 mM NaCl, 50 mM TRIS HCl pH 8.5 mM EDTA, 0.01% SDS, 0.005% Sodium deoxycholate, Roche protease inhibitors, PMSF) for 10 min at 4°C. Mouse tissues were previously homogenized with T 25 digital ULTRA-TURRAX®. Samples were clarified 10 min at 13000 rpm at 4°C. For immunoblots, equal amounts of proteins from both whole-cell lysates were resolved by SDS–PAGE and blotted to nitrocellulose membranes.

Immunofluorescence.

Cultured cells were fixed 5 min at RT using PFA 2% then treated 10 min at RT using CSK buffer [100 mM NaCl, 300 mM sucrose, 3 mM MgCl2, 10 mM PIPES (pH 6.8)], 0.7%

Triton, and finally fixed again 5 min at RT using PFA 2%. Mice were anaesthetized by using a mixture of Rompun/Zoletil and trans-cardially perfused with fixative solution (4% paraformaldehyde in PBS). Tumors were post-fixed overnight at 4°C, slowly dehydrated with increasing concentrations of Sucrose, embedded with Tissue-TEK (O.C.T, Sakura Finetek, Alphen aan den Rijn, The Netherlands), and frozen by using isopentane. 20µm cryo-sections were rehydrated in PBS before further processing. Cells and sections were permeabilized in 0.1% Triton X 100 in PBS for 10 min, saturated in 5% BSA in PBS for 30 min and incubated with a primary antibody for 1h at RT. Primary antibodies were detected with anti-rabbit Alexa Fluor 488 or 568 (Molecular Probes, Invitrogen), anti-mouse Alexa Fluor 488 or 568 (Molecular Probes, Invitrogen) used at 1:500 dilution for 30 min. Cells were counterstained with 0.5 µg/mL DAPI for 10 min and washed with PBS. TUNEL assay was performed 48h post transfection using the TMR red *In Situ* Cell Death Detection Kit (Roche, West Sussex, UK), according to manufacturer protocol. Images were acquired using an ApoTome system (Zeiss, Oberkochen, Germany) or using a Leica TCS SP5 confocal system (Leica Microsystems) equipped with a 405-nm diode, an argon ion, and a 561-nm DPSS laser.

Detection of senescent cells.

Senescent cells in cultures or in xenograft tumors were detected using in situ β-galactosidase staining, following the protocol reported described in (52)

Immunohistochemistry

Periodate-lysine-paraformaldehyde (PLP)-fixed and paraffin-embedded tissue sections were stained with haematoxylin & eosin (H&E). For immunohistochemistry assays, de-waxed 5 µm sections were submitted to wet heat-induced antigen retrieval in a mixture of 0.1M Tris and 0.01M EDTA solution at pH 9.0. Endogenous peroxidase was blocked in 0.6% hydrogen peroxide solution in 0.05M TBS (pH 7.6) for 20 min at room temperature.

Sections were then treated with 5% normal goat serum and reacted overnight with antibodies. Subsequently, sections were incubated with goat anti-rabbit (ab97051; Abcam) or anti-mouse (ab97240; Abcam) IgG conjugated to HRP for 1h at room temperature. Finally, sections were treated with diaminobenzidine enhanced liquid substrate chromogen system (D3939; Sigma-Aldrich) and counterstained with haematoxylin. Apoptosis was assessed using In Situ Cell Death Detection Kit POD (Roche) according to manufacturer's instructions.

Tamoxifen treatment

In all in vivo experiments, littermate mice, homozygous for the Cit^{flox} allele, homozygous for the ND2:SmoA1 and possessing (iCRE+) or non-possessing (iCRE-) the ER^{T2} allele were treated for five days with 0.100mg/g of tamoxifen by intraperitoneal injection.

Survival analysis

Kaplan–Meier method was used to estimate survival. For tamoxifen-treated mice, two months-old littermates, divided in iCRE+ and iCRE- cohorts, were treated and monitored for health status and movement abnormalities. All mice were euthanized at the onset of symptoms, including 10% weight loss, ataxia, or lethargy.

To analyze human MB patients survival in function of CITK expression, raw data of Gene Expression Omnibus (GEO) dataset GSE85217 (33), generated on Affymetrix Human Gene 1.1 ST Array platform, were downloaded and normalized through RMA algorithm as in Bioconductor oligo package (53). Mapping of Affy IDs to transcripts was based on NetAffx annotation (release na36, hg19). To specifically focus the analysis on CITK and exclude CITN isoform expression, we selected kinase domain probe-sets (7966920, 7966921, 7966922, 7966923, 7966924, 7966925, 7966926, 7966927) and averaged the corresponding expression values in each sample. Overall Survival data were obtained from (33) and maximal survival time was cut at 15 years. Patients were divided in two

groups using median expression as the discriminant value. In both cases, statistical significance was set to p=0.05. Log-rank (Mantel-Cox) test was used to compare survival between experimental groups.

Magnetic Resonance Imaging (MRI)

Magnetic Resonance images were acquired at 7.1 T using a Bruker Avance 300 spectrometer. The animals were scanned weekly, starting from 8 weeks of age, in order to check the presence of tumors through T2-weighted (T2w) images acquired with the following parameters: Repetition Time (TR) = 4000 ms; Echo Time (TE) = 59 ms; Rare Factor (RF) = 24; slice thickness = 1 mm; 15 slices; field of view = 3.00 cm; matrix = 256 × 256; number of averages (NAV) = 4; total imaging time = 2m40s). Animals bearing a tumor mass (size 5 to 20mm^3) were then imaged with a high resolution Turbo-Rare sequence (TR = 2500 ms, TE = 36 ms, RF = 8, slice thickness = 0.5 mm; 20 slices; field of view = 3.50 cm; matrix = 384 × 384; NAV = 10; total imaging time = 20 min) before and 7,14, 21, 28 days after tamoxifen administration, to monitor tumor progression. Before undergoing MRI animals were anesthetized by intramuscular injection of 5 mg/kg of xylazine (Rompun; Bayer, Milan, Italy) and 20 mg/kg of tiletamine/zolazepam (Zoletil 100; Virbac, Milan, Italy). Tumor volume was assessed in each animal through MR data analysis, carried out with Bruker Paravision 5.1 Software. More in details, the tumor area was delineated in each slice of T2w high resolution images by manually drawing regions of interest along tumor borders. The tumor volume in each slice was estimated multiplying each tumor area for the slice thickness (0.5 mm). Finally, the total tumor volume was estimated by adding up all the single slice volumes.

Statistical analysis

Statistical analyses were performed using Microsoft Office Excel or Graphpad. Unpaired two-tails Student's t-test was used if not otherwise specified. The mean values shown

represent the average of at least three independent experiments and error bars are standard errors of the mean.

Results

SHH medulloblastoma cells are sensitive to CITK knock-down.

To investigate the dependence of SHH MB on CITK expression, we resorted to DAOY and ONS-76 cells, two established human MB lines showing a transcription profile typical of SHH activation (1), and carrying mutated or wild type TP53, respectively (54). We induced transient CITK knock-down in these cells (Fig. 1A) using two validated siRNA sequences (31) and analyzed CITK associated cellular phenotypes 48 hours after transfection. CITK loss induced apoptosis in both cell lines, as shown by high levels of cleaved Caspase-3 and Caspase-7 (Fig. 1A-B), as well as by increased rate of annexin V-positive cells (Fig. 1C) and of TUNEL-positive cells (Fig. 1D). In addition, after CITK knock down, both lines showed increased rate of binucleated cells, indicative of cytokinesis failure (Fig. 1E and (34)). We previously demonstrated that RNAi of CITK in ONS-76 cells leads to accumulation of DNA double strand breaks (DSB), as shown by higher frequency of γH2AX- and TP53BP1-positive nuclear foci and, most importantly, by gain of chromosome breaks (34). Accordingly, we found that also DAOY cells have increased frequency of γH2AX nuclear foci after CITK knock-down (Fig. 2A). Interestingly, in both cell lines, transfection of the two CITK-specific siRNA sequences significantly enhanced the proportion of cells in G0/G1 (Fig. 2B-C). This result suggests that, besides inducing cytokinesis failure, CITK loss reduces the number of MB cells that progress into S-phase and mitosis. Consistent with this observation, CITK-interfered ONS-76 and DAOY cells showed high levels of the cyclin-kinase inhibitors CDKN1A (P21) and CDKN1B (P27) (Fig. 2D-E).

Previous work has shown that CITK loss may elicit both TP53-dependent and TP53-independent effects (34,46). Accordingly, TP53 knock-down reverted to a great extent the apoptotic phenotype resulting from CITK RNAi in ONS-76 cells but had little effect in CITK-interfered DAOY cells (Fig. 3A-B). Since we previously showed that CITK loss increases TP73 RNA levels independently of the TP53 status (34), we assessed whether TP73 is involved in phenotypes produced by CITK loss in DAOY cells. As expected, TP73 protein levels are significantly increased in DAOY cells after CITK RNAi (Fig. 3C and 3D). Moreover, when the induction of TP73 was prevented by RNAi (Fig. 3C and 3D), apoptosis levels were significantly reduced (Fig. 3E) and the induction of growth arrest markers was not observed (Fig. 3C and 3F). Interestingly, TP53 or TP73 knock-down induced by itself a moderate increase of apoptosis levels. Taken together, these observations suggest that SHH MB cells are highly sensitive to CITK loss, which increases the frequency of DNA damage and cytokinesis failure and leads to apoptosis and cell cycle-progression block via TP53 or TP73.

Stable CITK knock-down impairs the expansion of SHH medulloblastoma cells *in vitro* and in xenograft assays.

To better evaluate the impact of CITK loss on SHH MB cells' growth, we generated DAOY and ONS-76 cell lines conditionally expressing control and CITK-specific shRNAs. To this aim, we cloned previously validated CITK sequences into a tightly regulated lentiviral-based system, in which shRNA expression can be induced by doxycycline administration (51) (Fig. S1A). Polyclonal populations obtained from both MB cell lines showed efficient CITK knockdown 48 hours after doxycycline administration (Fig. S1B). Stable knock-down of CITK recapitulated all the phenotypes produced by transient one (Fig. S1C-D). Furthermore, in long term colony forming assay, both DAOY and ONS-76 cells showed reduced growth rates compared to controls, after CITK shRNA induction by continuous

exposure to doxycycline (Fig. 4A-B). In addition, CITK knocked-down cells had a senescent morphology (Fig. 4C). Accordingly, CITK shRNA induction led to strong increase of cells positive for β-galactosidase cytochemical reaction (Fig. 4D), which is typical of senescent cells (52). To assess whether anti-proliferative effects of CITK loss are dependent on kinase activity, we used ONS-76 cells expressing CITK1 shRNA and performed rescue assays with overexpression vectors, coding for mouse CITK proteins. Interestingly, in CITK knocked down cells, transfection of RNAi-resistant wild type CITK (Fig. S1E) restored cell growth at control levels, while kinase-dead mutant did not revert the phenotype (Fig. 4E). This result indicates that CITK catalytic activity is required for SHH MB cells proliferation.

Next, we investigated whether CITK might be required for SHH MB cell expansion also *in vivo*, by performing xenograft assays with shRNA-expressing cell lines. In particular, considering the established malignant potential of DAOY cells and the higher effectiveness of the CITK1 sequence, we subcutaneously injected into immunodeficient mice DAOY cells, transduced with inducible control or with CITK1 shRNAs-containing lentiviruses. In mice fed with doxycycline-free diet, palpable tumors developed within six weeks after injection and underwent rapid growth afterwards (Fig. 5A). Continuous doxycycline administration had no significant effects on growth of tumors expressing control shRNA (Fig. 5A). In contrast, treatment reduced significantly the growth of CITK1 shRNA-expressing tumors (Fig. 5A-C). Interestingly, tumors expressing CITK1 shRNA showed also higher positivity to β-galactosidase staining, if compared to controls (Fig. 5D). Taken together, these results suggest that the inhibition of CITK impairs growth and induces cell senescence in SHH MB cells independently of TP53 status, both *in vitro* and *in vivo*.

CITK inactivation inhibits SHH-medulloblastoma progression.

CITK is not frequently mutated in human cancers (46) but is overexpressed in different tumor types (43–45), while it is expressed at very low levels in normal brain (55,56). By re-analyzing gene expression data of a recently published MB cohort (33), we found that tumors expressing CITK at levels higher than median have worse prognosis (Fig. S2A). We therefore asked whether CITK loss-of-function may elicit anti-neoplastic effects in patient-like MB. To this aim, we set out to induce CITK inactivation in tumors arising in the cerebellum of SmoA1 transgenic mice (57). This line expresses a constitutively active form of Smoothened gene (*Smo*) in cerebellar GNPs under the control of *NeuroD2* promoter (57) and shows, especially when crossed to homozygosity, high incidence of MB, closely mimicking the human disease (58). SmoA1 MB show high expression of CITK, if compared to the levels observed during normal cerebellar development (Fig. S2B). To inactivate CITK in these tumors in a temporally-controlled manner, we developed a mouse conditional *CitK* allele, in which the third exon is flanked by LoxP sites ($CitK^{flox}$, Fig. S3A). We then crossed this allele to homozygosity into transgenic mice constitutively expressing a tamoxifen-inducible $ER^{T2}CRE$ enzyme from Rosa26 locus (59). We assessed the effectiveness of conditional deletion by analyzing the ratio between recombined and non-recombined alleles (Fig. S3B), as well as CITK protein levels (Fig. S3C), in tissues of mice homozygous for $CitK^{flox}$ ($CitK^{flox/flox}$) and heterozygous for $ER^{T2}CRE$, treated with tamoxifen at postnatal day (P)60. Recombination of the $CitK^{flox}$ allele was efficiently induced by tamoxifen in lymphoid tissues (Fig. S3B-C). No significant histological differences were observed in thymus and spleen of CITK-deleted and control mice (Fig. S3D). One year follow up of a cohort of such mice did not show significant survival differences or pathologic abnormalities between treated $ER^{T2}CRE$ - and $ER^{T2}CRE$+ $CitK^{flox/flox}$ mice (data not shown). CITK deletion was not detected in mature brain (Fig. S3B), which mostly expresses the kinase domain-lacking isoform CITN (56) (Fig. 6A). However, since

effectiveness of tamoxifen-induced recombination could depend on proliferative activity or differentiation-related phenomena, we crossed the above mice with the SmoA1 line, to generate mice homozygous for SmoA1 and $CitK^{flox}$ alleles, and either ER^{T2}CRE-negative (control, iCRE-) or ER^{T2}CRE-positive (iCRE+). Under basal conditions, both iCRE- and iCRE+ mice developed MB, with similar frequency and in comparable times as SmoA1 transgenic mice (data not shown). To evaluate whether CITK could be inactivated in these tumors, as well as the effects of CITK acute loss, we injected tamoxifen for 5 consecutive days in mice showing at MRI MB of similar size (3-20 mm^3 diameter) and analyzed them 5 days after the last injection. Western blot analysis confirmed that tamoxifen treatment is effective in blunting CITK expression in iCRE+ tumors, but not in iCRE- controls (Fig. 6A). DNA analysis confirmed the effectiveness of recombination, but also showed that a significant fraction of cells in the tumors did not undergo CRE-mediated deletion (Fig. S3E). Nevertheless, tamoxifen-treated iCRE+ tumors showed increased levels of γH2AX, P21, P27 and P16, as well as cleaved Caspase-3 and Caspase-7 (Fig.6A-B). These results confirm that CITK loss leads to increased DNA damage, apoptosis and cell senescence in MB. Histopathological analysis revealed striking differences in cellular organization between tamoxifen-treated iCRE- and iCRE+ tumors. In iCRE- tumors, cells showed a whorl-packed-like arrangement organization (Fig. 6C); it is interesting to note the high number of macrophagic cells phagocitying apoptotic cell debries giving a pattern of “starry sky”, as it was reported in tumors with high proliferative index like Burkitt’s Lymphoma (60). In contrast, the morphological structure of tamoxifen-treated iCRE+ tumors was more heterogeneous, characterized by areas of packed small cells interleaved by areas of low cellular density (Fig. 6C). Immunohistochemical analysis underlined that the latter cells express low levels of the proliferation marker Ki67 and high levels of P27 (Fig. 6C). In addition, in P27-positive cells of CITK-deleted tumors, P27 was mostly

localized in the nucleus, as it would be expected in senescent cells (61), while in CITK-proficient tumors it was found in the cytoplasm (Fig. 6D). Conversely, cells in dense areas were mostly Ki67-positive and P27-negative (Fig. 6C). Consistent with biochemical data, we observed increased frequency of TUNEL-positive cells in sections of iCRE+ tumors (Fig. 6E).

To assess the overall anti-tumor effect of *CitK* deletion, we monitored tumor growth by MRI, before and after tamoxifen administration. This analysis showed that CITK loss impairs MB growth during the first four weeks after treatment (Fig. 7 A-B). In the end, we evaluated whether *CitK* deletion may significantly affect the survival of SmoA1 mice. To this aim, we treated with tamoxifen two months-old iCRE- and iCRE+ mice. At this stage more than 90% of SmoA1 homozygous mice are expected to develop sub-clinical tumors (58). Kaplan-Meier curves showed a significant increase in survival of the iCRE+ mice (Fig. 7C). Interestingly, western blot analysis of advanced tumors isolated from both groups revealed that all of them expressed similar levels of CITK, while the spleen of iCRE+ was still CITK-deficient (Fig. 7D).

Altogether, these results indicate that CITK deletion inhibits SmoA1 MB progression.

Discussion

In this report we explored the potential suitability of CITK as a target for MB therapy, by producing transient or stable RNAi-mediated knockdown in human MB cell lines, as well as temporally-controlled genetic inactivation in mouse MB of SmoA1 transgenic model. Data obtained in human MB cells confirmed that CITK is necessary for their *in vitro* expansion and that CITK loss leads to high frequency of cytokinesis failure and apoptosis, similarly to what has previously been described in developing neural progenitors (26,40) and in non-neural tumor cell lines (31,45,46,62). We also confirmed that DNA damage is a

prominent consequence of CITK loss (34). Interestingly, the strongest effect produced by CITK knock-down on cell cycle profile, was an increase in the proportion of G0/G1 cells, suggestive of high frequency of cell cycle arrest. This finding was partially unexpected, since previous studies in tumor cell lines (46,62) and in *CitK* knockout mice (26) reported an increase of G2/M or binucleated cells as the main alteration, correlating with high frequency of cytokinesis failure. Considering the change of cell morphology, as well as the increased positivity for β-galactosidase and the strong induction of cyclin kinase inhibitors P21 and P27, we conclude that human MB cell lines respond to CITK loss mainly by undergoing growth arrest and senescence, although cytokinesis failure is also detectable. A combination of apoptosis and senescence may therefore be responsible for the reduced expansion of cells after CITK knock-down, both in culture and in xenograft assays. Interestingly, we observed a similar response in TP53-proficient ONS-76 cells and in DAOY cells, expressing non-functional TP53, supporting the notion that CITK loss may lead to both TP53 dependent and TP53 independent anti-proliferative responses (34,46). Functional studies (Fig. 3) confirmed that wild type TP53 is a crucial player of the phenotypes elicited by CITK loss, and suggest that its role may be at least partially compensated by TP73. It is worth noting that TP53 knock-down in DAOY cells and both TP53 or TP73 knock-down in ONS-76 cells moderately increased *per se* apoptosis levels. In the first case, the phenomenon could be justified by the oncogenic activity of a mutant TP53, as previously reported in other cancer cell lines (63). A possible explanation of the ONS-76 results could be instead that wild type TP53 or TP73 knock-down may increase apoptosis in these cells by increasing the frequency of catastrophic mitoses. However, more detailed studies are necessary to better understand this phenomenon.

Analysis of a large gene expression dataset of MB patients' revealed that CITK expression is associated with worse prognosis (Supplementary Fig. S2A), but we cannot exclude that

this correlation may indirectly depend on mitotic activity, since CITK expression is cell cycle-dependent (27).

To analyze the effects of CITK inactivation in tumors mimicking patients' MB, we resorted to the SmoA1 transgenic model (57), in which we engineered temporally-controlled *CitK* deletion. With regard to these experiments, it must be underscored that tamoxifen-induced *CitK* deletion was only partially effective, although it acutely abolished CITK expression. Nevertheless, after tamoxifen treatment, CITK-deleted tumors showed increased apoptosis, as well as morphological, immunohistochemical and biochemical changes highly suggestive of senescence induction. Accordingly, CITK-deleted tumors showed reduced growth rate. Moreover, and most importantly, mice in which CITK was deleted at a pre-clinical stage had significantly improved survival, compared to non-deleted littermates similarly treated with tamoxifen. At the end of the follow-up period, tumors that developed in tamoxifen-treated iCRE+ mice showed CITK protein levels similar to those of iCRE- tumors, further indicating that CITK-deleted MB cells have a selective disadvantage if compared to non-deleted cells. These results indicate that deletion of *CitK* may favorably affect the clinical outcome of primary SHH-MB. It will be interesting to test whether similar effects can be produced by inactivating CITK in models of type III and type IV MB. In addition, it will be important to assess whether combination of CITK inactivation and established anti-MB treatments could act synergistically to increase tumor cells' death.

Reduced growth rate of MB cells expressing shRNAs against CITK could be rescued by expression of wild type CITK, but not by the corresponding kinase-defective mutant, suggesting that CITK catalytic activity is permissive for MB growth. Little is known about the CITK substrates that may be important for this activity. Myosin light chain, initially proposed as potential substrate, was not supported by in vivo evidence (64). Presently, the only bona-fide CITK substrate is the mitotic protein INCENP (65) but it is unknown whether

CITK-dependent INCENP phosphorylation may affect genomic stability. CITK is capable of interacting with different proteins linked to the accumulation of DNA damage such as P27 (66), ASPM (28), CK2α (50) and RAD51 (34), but it is still unknown whether some of these partners are direct substrates.

Nevertheless, based on the present results, as well as on finding that microcephaly patients with homozygous CITK null mutations or kinase-inactivating mutations show overlapping clinical phenotypes (40), we expect that CITK specific inhibitors should induce in MB biological responses resembling those produced by CITK loss of function. The development of such molecules will therefore represent a crucial topic for future research.

Authors' contributions: G. P., F. D. C. contributed for conception and design of the experiments; M.F developed the inducible cell lines; G. P., F. S, F.G., V. B., G. E. B., M. Fi. performed experiments and acquired data. G. P., F. S., F. T. B., U.A., M. G., A.M.A.C. analyzed and interpreted data. Writing, review and revision of the manuscript by G. P., F.D.C. and study supervision by J.C.C., E. Te., E. Tu., F.D.C.

Acknowledgements

We thank Dr. Luigi Varesio (Gaslini Hospital, Genova) for providing us with ONS-76 cells. We also thank Damiana Sattanino for technical assistance. This work was mainly supported by Associazione Italiana per la Ricerca sul Cancro (AIRC) with grant IG17527 to FDC. GP and VB were supported by a PhD fellowship from Italian Ministry of University and Research (MIUR). FG was supported by the Fondazione Umberto Veronesi fellowship program. The contribution of "Progetto ricerca locale Ex 60%" from University of Torino and of the EPIGEN flagship project from CNR to FDC is also gratefully acknowledged.

References

1. Triscott J, Lee C, Foster C, Manoranjan B, Pambid MR, Berns R, et al. Personalizing the treatment of pediatric medulloblastoma: Polo-like kinase 1 as a molecular target in high-risk children. Cancer Res. 2013;73:6734–44.
2. Cho Y-J, Tsherniak A, Tamayo P, Santagata S, Ligon A, Greulich H, et al. Integrative genomic analysis of medulloblastoma identifies a molecular subgroup that drives poor clinical outcome. J Clin Oncol Off J Am Soc Clin Oncol. 2011;29:1424–30.
3. Jones DTW, Jäger N, Kool M, Zichner T, Hutter B, Sultan M, et al. Dissecting the genomic complexity underlying medulloblastoma. Nature. 2012;488:100–5.
4. Kool M, Korshunov A, Remke M, Jones DTW, Schlanstein M, Northcott PA, et al. Molecular subgroups of medulloblastoma: an international meta-analysis of transcriptome, genetic aberrations, and clinical data of WNT, SHH, Group 3, and Group 4 medulloblastomas. Acta Neuropathol (Berl). 2012;123:473–84.
5. Northcott PA, Shih DJH, Peacock J, Garzia L, Morrissy AS, Zichner T, et al. Subgroup-specific structural variation across 1,000 medulloblastoma genomes. Nature. 2012;488:49–56.
6. Taylor MD, Northcott PA, Korshunov A, Remke M, Cho Y-J, Clifford SC, et al. Molecular subgroups of medulloblastoma: the current consensus. Acta Neuropathol (Berl). 2012;123:465–72.
7. Packer RJ, Vezina G. Management of and prognosis with medulloblastoma: therapy at a crossroads. Arch Neurol. 2008;65:1419–24.
8. Gajjar A, Packer RJ, Foreman NK, Cohen K, Haas-Kogan D, Merchant TE, et al. Children's Oncology Group's 2013 blueprint for research: central nervous system tumors. Pediatr Blood Cancer. 2013;60:1022–6.

9. Rutkowski S, von Hoff K, Emser A, Zwiener I, Pietsch T, Figarella-Branger D, et al. Survival and prognostic factors of early childhood medulloblastoma: an international meta-analysis. J Clin Oncol Off J Am Soc Clin Oncol. 2010;28:4961–8.
10. Gajjar A, Chintagumpala M, Ashley D, Kellie S, Kun LE, Merchant TE, et al. Risk-adapted craniospinal radiotherapy followed by high-dose chemotherapy and stem-cell rescue in children with newly diagnosed medulloblastoma (St Jude Medulloblastoma-96): long-term results from a prospective, multicentre trial. Lancet Oncol. 2006;7:813–20.
11. Moxon-Emre I, Bouffet E, Taylor MD, Laperriere N, Scantlebury N, Law N, et al. Impact of craniospinal dose, boost volume, and neurologic complications on intellectual outcome in patients with medulloblastoma. J Clin Oncol Off J Am Soc Clin Oncol. 2014;32:1760–8.
12. Palmer SL, Armstrong C, Onar-Thomas A, Wu S, Wallace D, Bonner MJ, et al. Processing speed, attention, and working memory after treatment for medulloblastoma: an international, prospective, and longitudinal study. J Clin Oncol Off J Am Soc Clin Oncol. 2013;31:3494–500.
13. Piscione PJ, Bouffet E, Mabbott DJ, Shams I, Kulkarni AV. Physical functioning in pediatric survivors of childhood posterior fossa brain tumors. Neuro-Oncol. 2014;16:147–55.
14. Ramaswamy V, Taylor MD. Medulloblastoma: From Myth to Molecular. J Clin Oncol Off J Am Soc Clin Oncol. 2017;35:2355–63.
15. Sengupta S, Pomeranz Krummel D, Pomeroy S. The evolution of medulloblastoma therapy to personalized medicine. F1000Research. 2017;6:490.

16. Oliver TG, Read TA, Kessler JD, Mehmeti A, Wells JF, Huynh TTT, et al. Loss of patched and disruption of granule cell development in a pre-neoplastic stage of medulloblastoma. Dev Camb Engl. 2005;132:2425–39.
17. Schüller U, Heine VM, Mao J, Kho AT, Dillon AK, Han Y-G, et al. Acquisition of granule neuron precursor identity is a critical determinant of progenitor cell competence to form Shh-induced medulloblastoma. Cancer Cell. 2008;14:123–34.
18. Yang Z-J, Ellis T, Markant SL, Read T-A, Kessler JD, Bourboulas M, et al. Medulloblastoma can be initiated by deletion of Patched in lineage-restricted progenitors or stem cells. Cancer Cell. 2008;14:135–45.
19. Samkari A, White J, Packer R. SHH inhibitors for the treatment of medulloblastoma. Expert Rev Neurother. 2015;15:763–70.
20. Gajjar A, Stewart CF, Ellison DW, Kaste S, Kun LE, Packer RJ, et al. Phase I study of vismodegib in children with recurrent or refractory medulloblastoma: a pediatric brain tumor consortium study. Clin Cancer Res Off J Am Assoc Cancer Res. 2013;19:6305–12.
21. Robinson GW, Orr BA, Wu G, Gururangan S, Lin T, Qaddoumi I, et al. Vismodegib Exerts Targeted Efficacy Against Recurrent Sonic Hedgehog-Subgroup Medulloblastoma: Results From Phase II Pediatric Brain Tumor Consortium Studies PBTC-025B and PBTC-032. J Clin Oncol Off J Am Soc Clin Oncol. 2015;33:2646–54.
22. Rudin CM, Hann CL, Laterra J, Yauch RL, Callahan CA, Fu L, et al. Treatment of medulloblastoma with hedgehog pathway inhibitor GDC-0449. N Engl J Med. 2009;361:1173–8.
23. Luo J, Solimini NL, Elledge SJ. Principles of cancer therapy: oncogene and non-oncogene addiction. Cell. 2009;136:823–37.

24. Di Cunto F, Calautti E, Hsiao J, Ong L, Topley G, Turco E, et al. Citron rho-interacting kinase, a novel tissue-specific ser/thr kinase encompassing the Rho-Rac-binding protein Citron. J Biol Chem. 1998;273:29706–11.
25. Madaule P, Eda M, Watanabe N, Fujisawa K, Matsuoka T, Bito H, et al. Role of citron kinase as a target of the small GTPase Rho in cytokinesis. Nature. 1998;394:491–4.
26. Di Cunto F, Imarisio S, Hirsch E, Broccoli V, Bulfone A, Migheli A, et al. Defective neurogenesis in citron kinase knockout mice by altered cytokinesis and massive apoptosis. Neuron. 2000;28:115–27.
27. Liu H, Di Cunto F, Imarisio S, Reid LM. Citron kinase is a cell cycle-dependent, nuclear protein required for G2/M transition of hepatocytes. J Biol Chem. 2003;278:2541–8.
28. Gai M, Bianchi FT, Vagnoni C, Vernì F, Bonaccorsi S, Pasquero S, et al. ASPM and CITK regulate spindle orientation by affecting the dynamics of astral microtubules. EMBO Rep. 2016;17:1396–409.
29. Bassi ZI, Verbrugghe KJ, Capalbo L, Gregory S, Montembault E, Glover DM, et al. Sticky/Citron kinase maintains proper RhoA localization at the cleavage site during cytokinesis. J Cell Biol. 2011;195:595–603.
30. D'Avino PP. Citron kinase - renaissance of a neglected mitotic kinase. J Cell Sci. 2017;130:1701–8.
31. Gai M, Camera P, Dema A, Bianchi F, Berto G, Scarpa E, et al. Citron kinase controls abscission through RhoA and anillin. Mol Biol Cell. 2011;22:3768–78.
32. Dema A, Macaluso F, Sgrò F, Berto GE, Bianchi FT, Chiotto AA, et al. Citron kinase-dependent F-actin maintenance at midbody secondary ingression sites mediates abscission. J Cell Sci. 2018;

33. Cavalli FMG, Remke M, Rampasek L, Peacock J, Shih DJH, Luu B, et al. Intertumoral Heterogeneity within Medulloblastoma Subgroups. Cancer Cell. 2017;31:737-754.e6.
34. Bianchi FT, Tocco C, Pallavicini G, Liu Y, Vernì F, Merigliano C, et al. Citron Kinase Deficiency Leads to Chromosomal Instability and TP53-Sensitive Microcephaly. Cell Rep. 2017;18:1674–86.
35. Ackman JB, Ramos RL, Sarkisian MR, Loturco JJ. Citron kinase is required for postnatal neurogenesis in the hippocampus. Dev Neurosci. 2007;29:113–23.
36. Di Cunto F, Imarisio S, Camera P, Boitani C, Altruda F, Silengo L. Essential role of citron kinase in cytokinesis of spermatogenic precursors. J Cell Sci. 2002;115:4819–26.
37. Sarkisian MR, Li W, Di Cunto F, D'Mello SR, LoTurco JJ. Citron-kinase, a protein essential to cytokinesis in neuronal progenitors, is deleted in the flathead mutant rat. J Neurosci Off J Soc Neurosci. 2002;22:RC217.
38. Basit S, Al-Harbi KM, Alhijji SAM, Albalawi AM, Alharby E, Eldardear A, et al. CIT, a gene involved in neurogenic cytokinesis, is mutated in human primary microcephaly. Hum Genet. 2016;135:1199–207.
39. Harding BN, Moccia A, Drunat S, Soukarieh O, Tubeuf H, Chitty LS, et al. Mutations in Citron Kinase Cause Recessive Microlissencephaly with Multinucleated Neurons. Am J Hum Genet. 2016;99:511–20.
40. Li H, Bielas SL, Zaki MS, Ismail S, Farfara D, Um K, et al. Biallelic Mutations in Citron Kinase Link Mitotic Cytokinesis to Human Primary Microcephaly. Am J Hum Genet. 2016;99:501–10.
41. Shaheen R, Hashem A, Abdel-Salam GMH, Al-Fadhli F, Ewida N, Alkuraya FS. Mutations in CIT, encoding citron rho-interacting serine/threonine kinase, cause severe primary microcephaly in humans. Hum Genet. 2016;135:1191–7.

42. Damasco C, Lembo A, Somma MP, Gatti M, Di Cunto F, Provero P. A signature inferred from Drosophila mitotic genes predicts survival of breast cancer patients. PloS One. 2011;6:e14737.
43. Ehrlichova M, Mohelnikova-Duchonova B, Hrdy J, Brynychova V, Mrhalova M, Kodet R, et al. The association of taxane resistance genes with the clinical course of ovarian carcinoma. Genomics. 2013;102:96–101.
44. Tong H, Wang J, Chen H, Wang Z, Fan H, Ni Z. Transcriptomic analysis of gene expression profiles of stomach carcinoma reveal abnormal expression of mitotic components. Life Sci. 2017;170:41–9.
45. Fu Y, Huang J, Wang K-S, Zhang X, Han Z-G. RNA interference targeting CITRON can significantly inhibit the proliferation of hepatocellular carcinoma cells. Mol Biol Rep. 2011;38:693–702.
46. McKenzie C, D'Avino PP. Investigating cytokinesis failure as a strategy in cancer therapy. Oncotarget. 2016;7:87323–41.
47. Whitworth H, Bhadel S, Ivey M, Conaway M, Spencer A, Hernan R, et al. Identification of kinases regulating prostate cancer cell growth using an RNAi phenotypic screen. PloS One. 2012;7:e38950.
48. Bianchi FT, Gai M, Berto GE, Di Cunto F. Of rings and spines: The multiple facets of Citron proteins in neural development. Small GTPases. 2017;1–9.
49. Caracciolo V, D'Agostino L, Dráberová E, Sládková V, Crozier-Fitzgerald C, Agamanolis DP, et al. Differential expression and cellular distribution of gamma-tubulin and betaIII-tubulin in medulloblastomas and human medulloblastoma cell lines. J Cell Physiol. 2010;223:519–29.

50. Sgrò F, Bianchi FT, Falcone M, Pallavicini G, Gai M, Chiotto AMA, et al. Tissue-specific control of midbody microtubule stability by Citron kinase through modulation of TUBB3 phosphorylation. Cell Death Differ. 2016;23:801–13.
51. Wiznerowicz M, Trono D. Conditional suppression of cellular genes: lentivirus vector-mediated drug-inducible RNA interference. J Virol. 2003;77:8957–61.
52. Dimri GP, Lee X, Basile G, Acosta M, Scott G, Roskelley C, et al. A biomarker that identifies senescent human cells in culture and in aging skin in vivo. Proc Natl Acad Sci U S A. 1995;92:9363–7.
53. Gentleman RC, Carey VJ, Bates DM, Bolstad B, Dettling M, Dudoit S, et al. Bioconductor: open software development for computational biology and bioinformatics. Genome Biol. 2004;5:R80.
54. Künkele A, De Preter K, Heukamp L, Thor T, Pajtler KW, Hartmann W, et al. Pharmacological activation of the p53 pathway by nutlin-3 exerts anti-tumoral effects in medulloblastomas. Neuro-Oncol. 2012;14:859–69.
55. Wang ET, Sandberg R, Luo S, Khrebtukova I, Zhang L, Mayr C, et al. Alternative isoform regulation in human tissue transcriptomes. Nature. 2008;456:470–6.
56. Di Cunto F, Ferrara L, Curtetti R, Imarisio S, Guazzone S, Broccoli V, et al. Role of citron kinase in dendritic morphogenesis of cortical neurons. Brain Res Bull. 2003;60:319–27.
57. Hallahan AR, Pritchard JI, Hansen S, Benson M, Stoeck J, Hatton BA, et al. The SmoA1 mouse model reveals that notch signaling is critical for the growth and survival of sonic hedgehog-induced medulloblastomas. Cancer Res. 2004;64:7794–800.

58. Hatton BA, Villavicencio EH, Tsuchiya KD, Pritchard JI, Ditzler S, Pullar B, et al. The Smo/Smo Model: Hedgehog-Induced Medulloblastoma with 90% Incidence and Leptomeningeal Spread. Cancer Res. 2008;68:1768–76.
59. Ventura A, Kirsch DG, McLaughlin ME, Tuveson DA, Grimm J, Lintault L, et al. Restoration of p53 function leads to tumour regression in vivo. Nature. 2007;445:661–5.
60. Chuang S-S, Ye H, Du M-Q, Lu C-L, Dogan A, Hsieh P-P, et al. Histopathology and immunohistochemistry in distinguishing Burkitt lymphoma from diffuse large B-cell lymphoma with very high proliferation index and with or without a starry-sky pattern: a comparative study with EBER and FISH. Am J Clin Pathol. 2007;128:558–64.
61. Hnit SST, Xie C, Yao M, Holst J, Bensoussan A, De Souza P, et al. p27(Kip1) signaling: Transcriptional and post-translational regulation. Int J Biochem Cell Biol. 2015;68:9–14.
62. Gruneberg U, Neef R, Li X, Chan EHY, Chalamalasetty RB, Nigg EA, et al. KIF14 and citron kinase act together to promote efficient cytokinesis. J Cell Biol. 2006;172:363–72.
63. Zhu H-B, Yang K, Xie Y-Q, Lin Y-W, Mao Q-Q, Xie L-P. Silencing of mutant p53 by siRNA induces cell cycle arrest and apoptosis in human bladder cancer cells. World J Surg Oncol. 2013;11:22.
64. Matsumura F. Regulation of myosin II during cytokinesis in higher eukaryotes. Trends Cell Biol. 2005;15:371–7.
65. McKenzie C, Bassi ZI, Debski J, Gottardo M, Callaini G, Dadlez M, et al. Cross-regulation between Aurora B and Citron kinase controls midbody architecture in cytokinesis. Open Biol. 2016;6.

66. Serres MP, Kossatz U, Chi Y, Roberts JM, Malek NP, Besson A. p27(Kip1) controls cytokinesis via the regulation of citron kinase activation. J Clin Invest. 2012;122:844–58.

Figures legends

Figure 1. CITK knockdown leads to apoptosis and cytokinesis failure in medulloblastoma cell lines.

(A) Western blot of total cell lysates obtained from DAOY and ONS-76 cells, treated for 48 hours with non-targeting (siCtrl) or CITK-specific (siCITK1, siCITK2) siRNA sequences. Levels of CITK and of cleaved forms of Caspase 3 (cC3) and 7 (cC7) were analyzed. Internal loading control was Vinculin (VINC).

(B) Quantification of the relative density of cC3 and cC7 in siCITK1 cells, compared to cells treated with siCtrl. (N=5).

(C) Quantification of annexin V positive DAOY and ONS-76 cells, 48h after transfection with siCtrl or with two different CITK-specific siRNA sequences (N=15).

(D) DAOY and ONS-76 cells were treated for 48 hours with siCtrl or siCITK1 and apoptotic cells were quantified. On the left, representative images of DAOY and ONS-76 analyzed with TUNEL (in red) and counterstained with DAPI. On the right, quantification of TUNEL positive cells.

(E) DAOY cells, seeded at low density, were processed for immunofluorescence 48h after transfection with non-targeting or CITK-specific siRNA sequences, and stained with DAPI and anti-alpha-tubulin antibodies. The percentage of binucleated cells was then assessed. All quantifications were based on three independent biological replicates, unless noted otherwise. Error bars = standard error of the mean. * $P < 0.05$, ** $P < 0.01$, *** $P < 0.001$, two tailed Student's T-test. Scale bars = 20 µm

Figure 2. Medulloblastoma cell lines accumulate DNA damage and arrest their cell cycle after CITK knock down.

(A) High magnification of DAOY cells treated treated for 48 hours with siCtrl or siCITK1, stained with the DNA-damage marker γH2AX and counterstained with DAPI. On the right, quantification of γH2AX foci per nucleus.

(B) Flow-cytometric analysis of DNA content in DAOY and ONS-76 cells, treated as in panel A.

(C) Quantification of diploid (G0-G1), S-phase and tetraploid (G2-M) cells distribution in experiments performed as in panel B. All the differences between CITK-specific siRNAs and controls were significant ($p < 10^{-7}$, Chi-square test performed assuming the null hypothesis that cell cycle distribution is independent on siRNAs condition).

(D) Western blot of total cell lysates obtained from DAOY and ONS-76 cells, treated as in panel A. Levels of P27 and P21 were analyzed. Internal loading control was Vinculin (VINC).

(E) Quantification of the relative intensity of P27 and P21 in western blot analysis performed as in panel D.

All quantifications were based on four independent biological replicates.

Error bars = standard error of the mean. * $P < 0.05$, ** $P < 0.01$, *** $P < 0.001$ (Mann-Withney U test for panel A, two tailed Student's T-test for blots). Scale bars = 20 μm

Figure 3. CITK loss in medulloblastoma cells induces TP53-dependent and TP53-independent response.

(A) Western blot of total cell lysates obtained from DAOY and ONS-76 cells, treated for 48 hours with the indicated siRNA sequences (+). Samples in which a specific targeting sequence was missing (-) were treated with same amount of non-targeting control sequence. Internal loading control was Vinculin (VINC).

(B) Quantification of annexin V positive DAOY and ONS-76 cells, 48h after transfection with the indicated siRNA sequences (N=at least to 8).

(C) Western blot of total cell lysates obtained from DAOY cells, treated for 48 hours with the indicated siRNA sequences.

(D) Quantification of the relative intensity of TP73 in western blot analyses performed as in panel C (N=4).

(E) Quantification of annexin V positive DAOY, 48h after transfection with the indicated siRNA sequences (N=at least 7).

(F) Quantification of the relative intensity of P27 and P21 in western blot analyses performed as in panel C (N=4).

Error bars = standard error of the mean. * $P < 0.05$, ** $P < 0.01$, *** $P < 0.001$, two tailed Student's T-test.

Figure 4. CITK loss decreases proliferation and induces senescence in medulloblastoma cell lines.

(A) DAOY and ONS-76 cells, stably transfected with inducible non targeting (shCtrl) or CITK-specific shRNA sequences (CITK1 and CITK2), were plated (5000 cells) in control medium (Vehicle) or in Doxycycline-containing (Doxy) medium (2 μM). Growth curves were then obtained by assessing cell number in dishes at the indicated times.

(B) DAOY and ONS-76 cells, expressing non targeting or CITK-specific shRNA sequences under Doxycycline-inducible control, were plated in 35 mm dishes (500cells/dish) 48 hours after shRNA induction with 2 μM Doxycycline. After additional 5 days of continuous exposure to Doxycycline, the obtained colonies were fixed and stained with crystal violet.

(C) Phase contrast images of representative fields, in cultures of DAOY and ONS-76 cells, expressing shCtrl or shCITK1, 5 days after doxycycline induction.

(D) Quantification of the percentage of β-Galactosidase positive colonies in cultures treated as in B, five days after doxycycline administration.

(E) ONS-76 cells, obtained as in B, were induced with doxycycline for 24 hours and then transfected with control vector (OE Myc) or with vectors over expressing mouse wild type (OE *CitK*) or Citron kinase inactive form (OE *CitKd*). Cell number in dishes was then quantified 24 hours later.

All quantifications were based on five independent biological replicates. Error bars = standard error of the mean. * $P < 0.05$, ** $P < 0.01$, *** $P < 0.001$, n.s. = non-significant, two tailed Student's T-test. Scale bars = 20 µm

Figure 5. CITK knock down decreases growth and induces senescence in DAOY xenograft tumors.

(A) DAOY cells stably transduced with the indicated shRNA vectors were injected subcutaneously in NOD-SCID mice. Tumor growth was monitored weekly. Doxycycline (Doxy) 10mg/ml or ethanol (Vehicle) was added to the drinking water six weeks after cells injection, and tumor growth was monitored for three additional weeks.

Analysis of xenograft tumors growth was performed by measuring subcutaneous tumor diameter.

(B) Quantification of tumor weight after explantation, performed at the end of the experiments described in A.

(C) Representative pictures of xenograft tumors, obtained after explantation at the end of the experiments described in A.

(D) Representative pictures of xenograft tumors obtained from doxycycline-treated mice and stained with β-galactosidase assay.

All quantifications were based on seven independent biological replicates. Error bars = standard error of the mean. * P < 0.05, ** P < 0.01, two tailed Student's T-test. Scale bars = 50 mm.

Figure 6. Loss of CITK leads to senescence and apoptosis in primary medulloblastoma.

(A) Western blot analysis, performed with indicated antibodies, of total cell lysates obtained from MB explanted from mice homozygous for SmoA1 transgene and for conditional $CitK^{flox}$ allele, and either negative (iCRE-) or positive (iCRE+) for ERT2Cre allele, whose activity was induced by tamoxifen treatment (5 days 0.100mg/g). Explants were obtained 5 days after the last tamoxifen injection. Results of two independent tumors per each genotypes are shown. cC3 and cC7 represent cleaved Caspase 3 and 7, respectively. Internal loading control was Vinculin (VINC). Note that the anti-CIT antibodies recognize both CITK and CITN isoforms.

(B) Quantification of the ratio between signals obtained in iCRE+ and iCRE- mice, in experiments performed as described in A.

(C) Paraffin sections from tumors obtained as in panel A were analyzed by histology using H&E staining, as well as by immunohistochemistry with antibodies anti Ki67 and P27 antigens. Immunohistochemistry samples were counterstained with hematoxylin.

(D) Frozen sections of MB obtained as in A were processed for immunofluorescence, stained using anti P27 antibodies and counterstained with DAPI. Note the nuclear accumulation of P27 in iCRE+ tumors.

(E) TUNEL staining (brown nuclei) of paraffin sections obtained as in panel A, counterstained with hematoxylin and quantification of TUNEL positive cells.

All western blot quantifications were based on five independent biological replicates. Immunohistochemistry analysis and TUNEL quantification based on three independent

biological replicates. Error bars = standard error of the mean. * P < 0.05, ** P < 0.01, *** P < 0.001, two tailed Student's T-test. Scale bars = 30 µm.

Figure 7. *CitK* deletion reduces MBs progression and increases SmoA mice survival.

(A) Representative T2 weighted MRI-based follow up of MB originating in iCRE- or iCRE+ mice at different time points after tamoxifen treatment (time 0). Original images in grayscale as well as pseudo-colorized images are displayed; red and yellow lines outline the tumor area in MRI sections.

(B) Quantitative analysis of tumor growth, in follow up experiment performed as described in panel A. Tumor volumes were reconstructed summing up the corresponding voxels in each section (N=6). Error bars = standard error of the mean. * P < 0.05, ** P < 0.01, two tailed Student's T-test.

(C) Kaplan-Meier survival curves of control (iCRE-) and CITK-deleted (iCRE+) mice, treated for 5 days with tamoxifen at 9 weeks of age (N=at least 30). Log-rank (Mantel-Cox) test was used to compare survival between experimental groups.

(D) Western blot analysis of CITK levels, in cell lysates obtained from control (iCRE-) and CITK-deleted (iCRE+) tumors, explanted one week or 28 weeks after the end of tamoxifen treatment. Internal loading control was beta actin (ACTB).

Figure 1

Pallavicini et al.

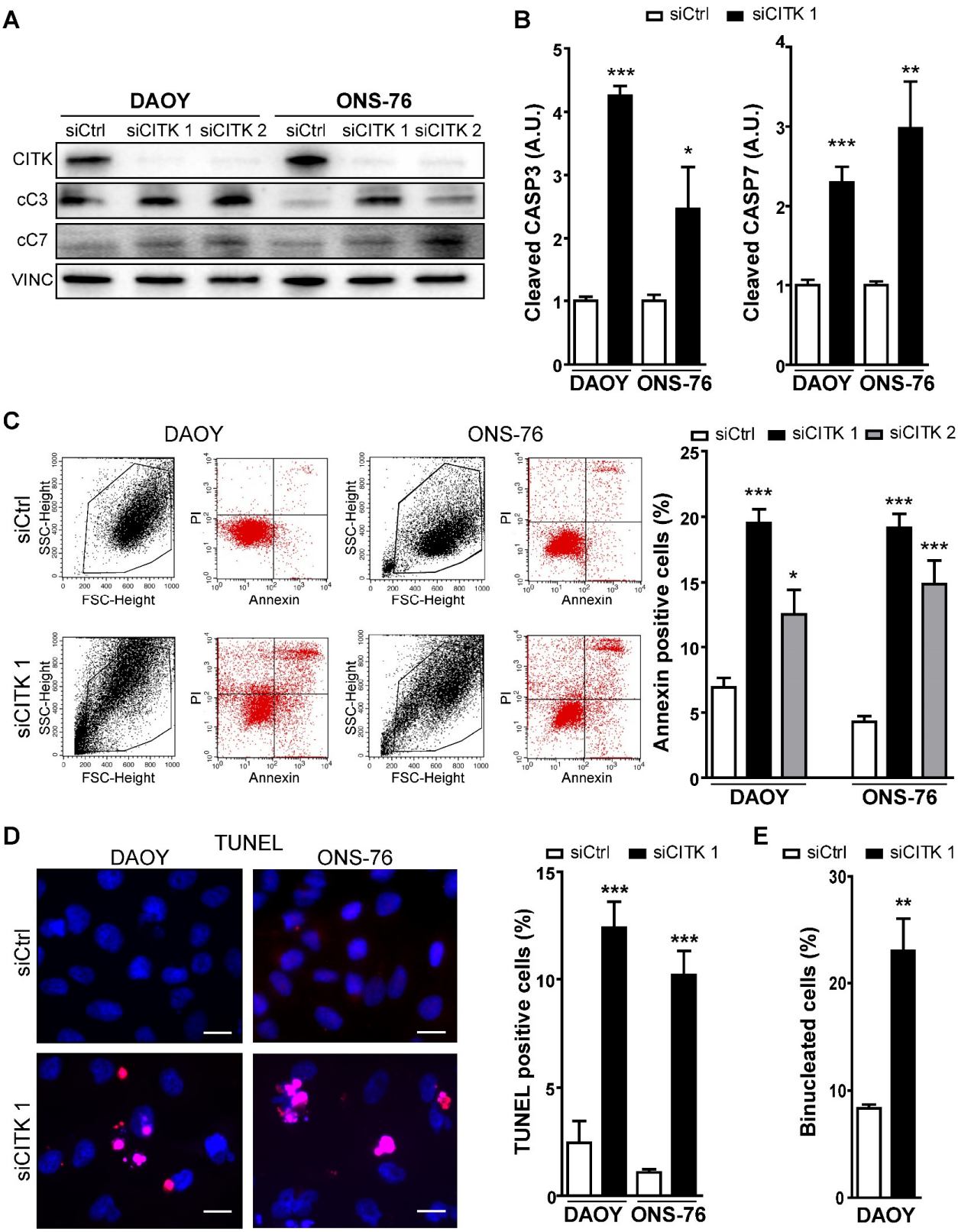

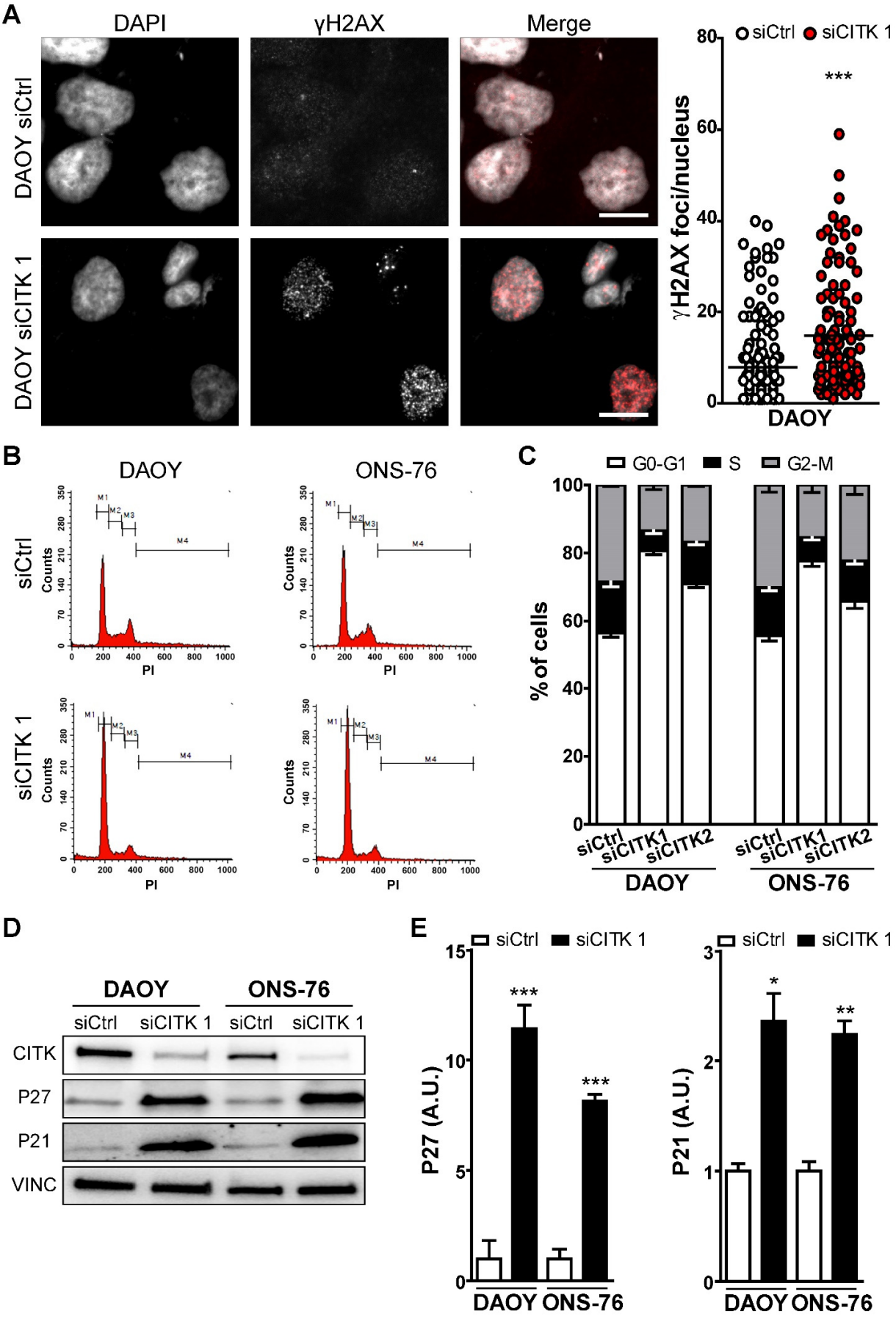
A
DAPI
γH2AX
Merge
DAOY siCtrl
DAOY siCITK 1
siCtrl
siCITK 1
***
γH2AX foci/nucleus
DAOY
B
DAOY
ONS-76
siCtrl
siCITK 1
Counts
PI
C
G0-G1
S
G2-M
% of cells
siCtrl
siCITK1
siCITK2
DAOY
ONS-76
D
DAOY
ONS-76
siCtrl
siCITK 1
CITK
P27
P21
VINC
E
P27 (A.U.)
P21 (A.U.)
*
**

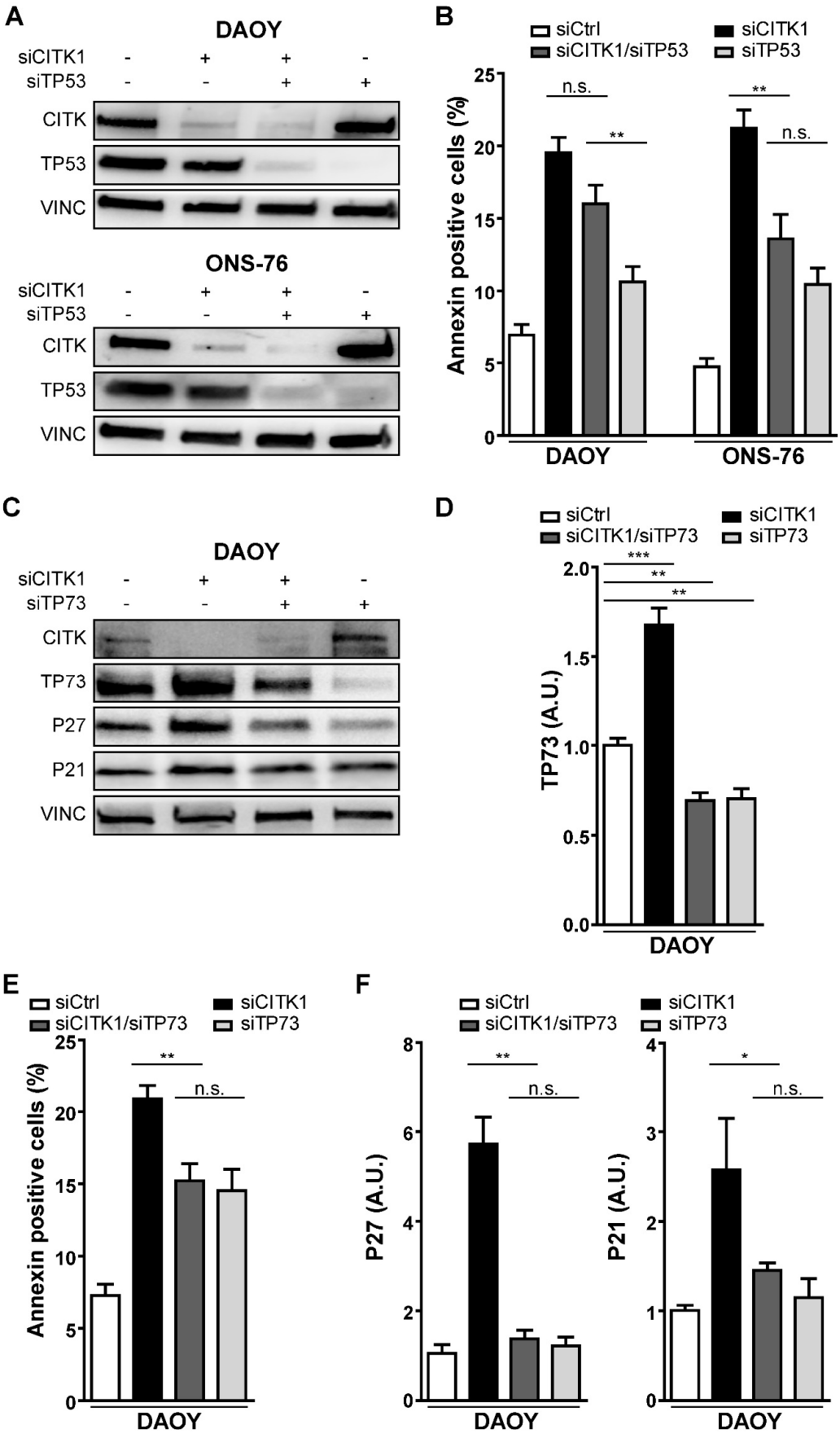
A
DAOY
siCITK1 - + + -
siTP53 - - + +
CITK
TP53
VINC
ONS-76
siCITK1 - + + -
siTP53 - - + +
CITK
TP53
VINC
B
siCtrl
siCITK1/siTP53
siCITK1
siTP53
Annexin positive cells (%)
n.s.
**
**
n.s.
DAOY
ONS-76
C
DAOY
siCITK1 - + + -
siTP73 - - + +
CITK
TP73
P27
P21
VINC
D
siCtrl
siCITK1/siTP73
siCITK1
siTP73
***
**
**
TP73 (A.U.)
DAOY
E
siCtrl
siCITK1/siTP73
siCITK1
siTP73
Annexin positive cells (%)
**
n.s.
DAOY
F
siCtrl
siCITK1/siTP73
siCITK1
siTP73
**
n.s.
P27 (A.U.)
DAOY
*
n.s.
P21 (A.U.)
DAOY

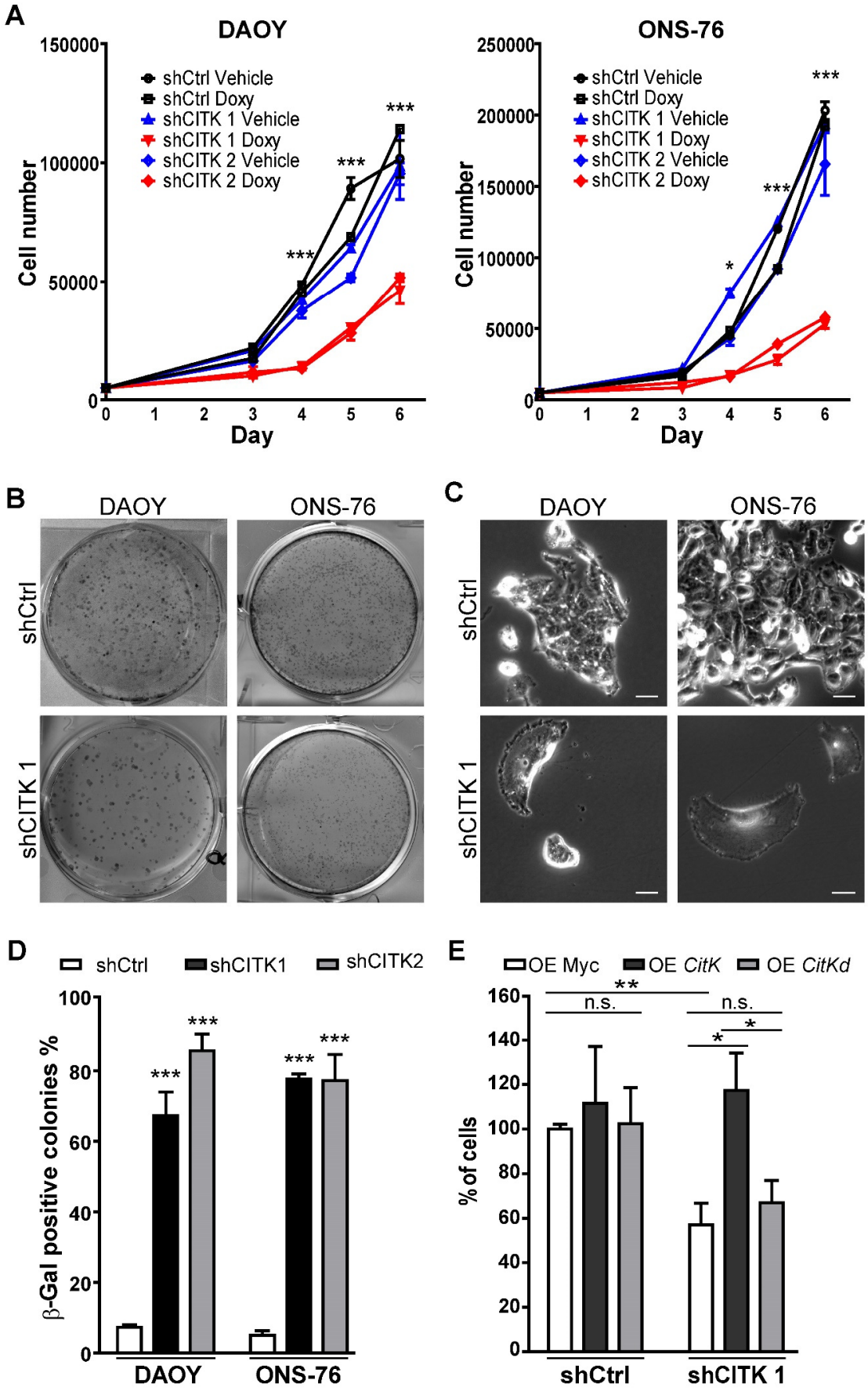
A
DAOY
ONS-76
shCtrl Vehicle
shCtrl Doxy
shCITK 1 Vehicle
shCITK 1 Doxy
shCITK 2 Vehicle
shCITK 2 Doxy
Cell number
Day
B
DAOY
ONS-76
shCtrl
shCITK 1
C
DAOY
ONS-76
shCtrl
shCITK 1
D
shCtrl
shCITK1
shCITK2
β-Gal positive colonies %
DAOY
ONS-76
E
OE Myc
OE CitK
OE CitKd
% of cells
n.s.
shCtrl
shCITK 1

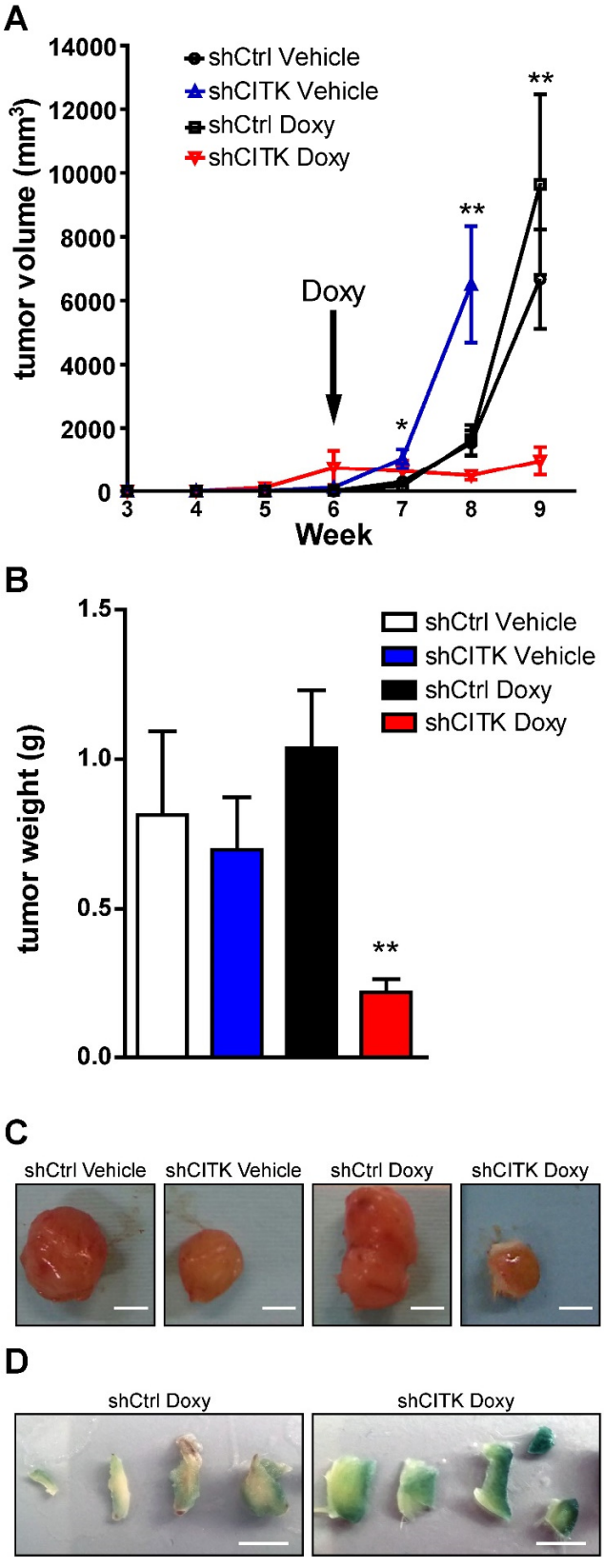
A
14000
12000
10000
8000
6000
4000
2000
0
tumor volume (mm3)
shCtrl Vehicle
shCITK Vehicle
shCtrl Doxy
shCITK Doxy
Doxy
*
**
**
3
4
5
6
7
8
9
Week
B
1.5
1.0
0.5
0.0
tumor weight (g)
shCtrl Vehicle
shCITK Vehicle
shCtrl Doxy
shCITK Doxy
**
C
shCtrl Vehicle
shCITK Vehicle
shCtrl Doxy
shCITK Doxy
D
shCtrl Doxy
shCITK Doxy

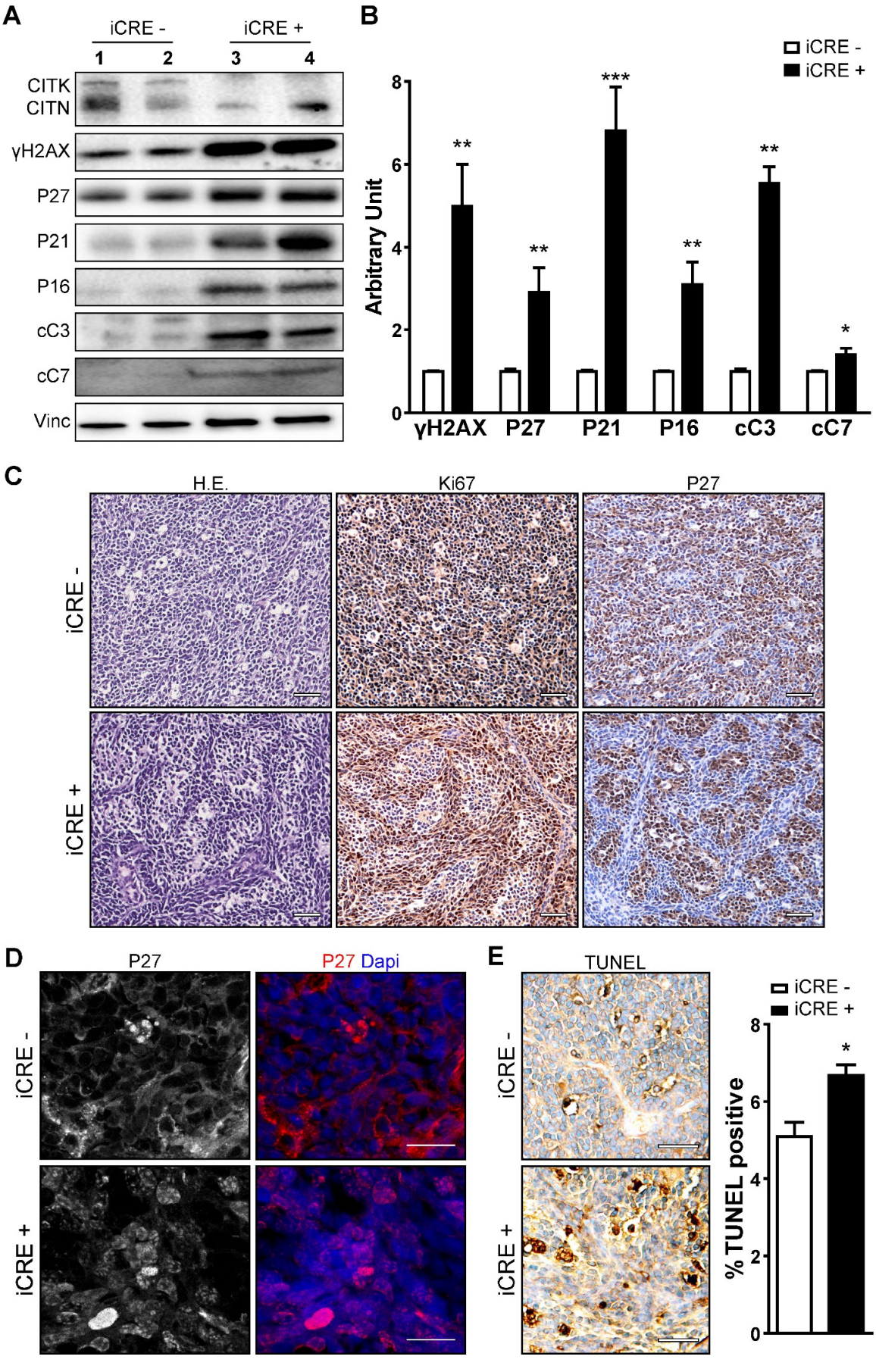
A
iCRE -
iCRE +
1
2
3
4
CITK
CITN
γH2AX
P27
P21
P16
cC3
cC7
Vinc
B
iCRE -
iCRE +
Arbitrary Unit
γH2AX
P27
P21
P16
cC3
cC7
C
H.E.
Ki67
P27
iCRE -
iCRE +
D
P27
P27 Dapi
iCRE -
iCRE +
E
TUNEL
iCRE -
iCRE +
% TUNEL positive

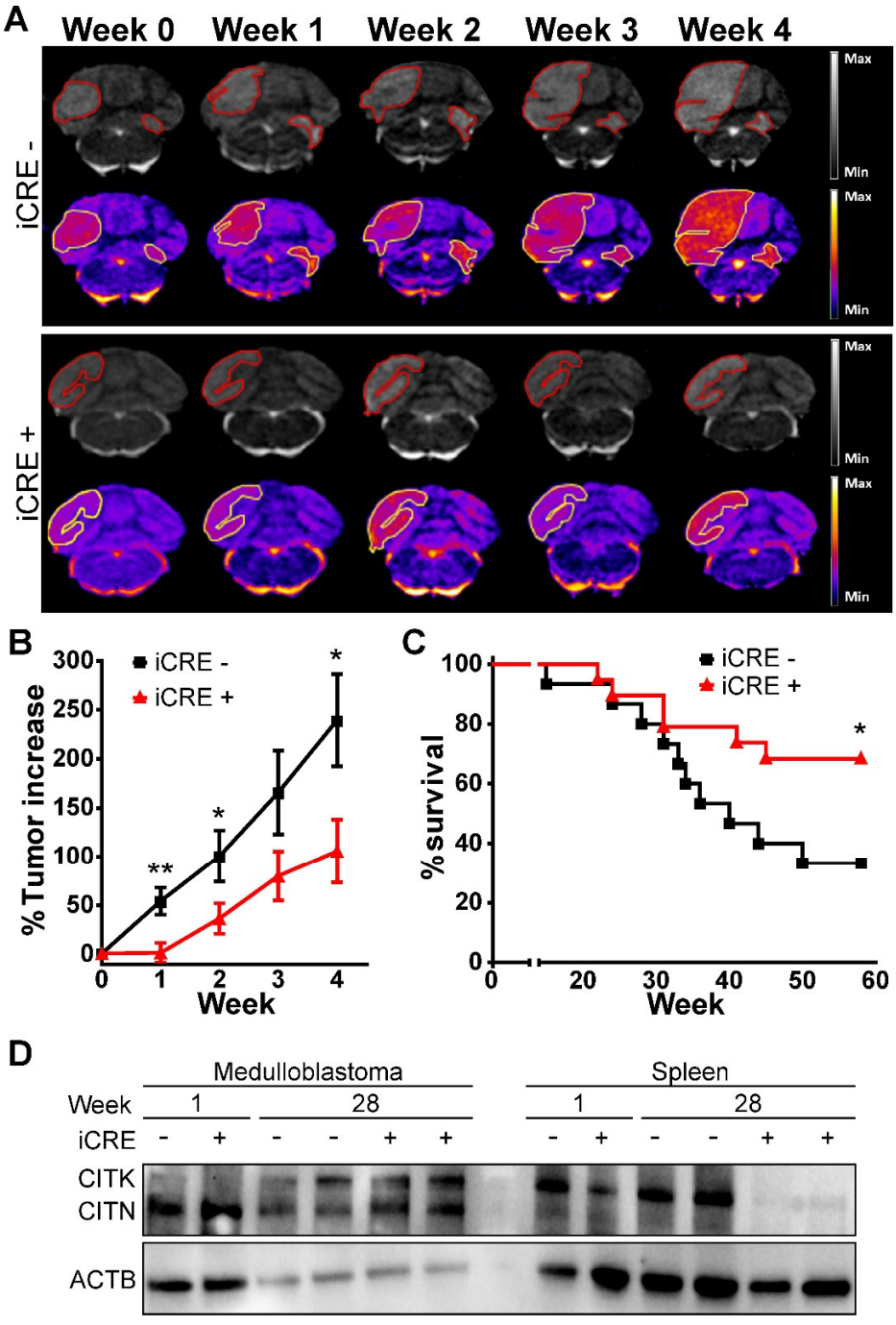
A
Week 0
Week 1
Week 2
Week 3
Week 4
iCRE -
iCRE +
Max
Min
B
% Tumor increase
iCRE -
iCRE +
Week
C
% survival
iCRE -
iCRE +
Week
D
Medulloblastoma
Spleen
Week
iCRE
CITK
CITN
ACTB